Control and Power Sharing of an Islanded DC Microgrid Integrating a Back-up Diesel Generator

Elie Hleihel, Maurice Fadel, Hadi Y. Kanaan

Control and Power Sharing of an Islanded DC Microgrid Integrating a Back-up Diesel Generator

Elie Hleihel[1,2], Maurice Fadel[1] and Hadi Y. Kanaan[2]
[1]Université de Toulouse, LAPLACE, 2 rue Charles Camichel 31071 Toulouse cedex 7
[2]Saint-Joseph University of Beirut, Faculty of Engineering – ESIB, Mar Roukoz, Mkalles, Beirut, Lebanon
hleihel@laplace.univ-tlse.fr, maurice.fadel@laplace.univ-tlse.fr, hadi.kanaan@usj.edu.lb

***Abstract*- Originally proposed at the beginning of the twenty-first century, as a solution to electrify remote areas and integrate renewable energy sources to mitigate environmental pollution, Microgrids are gaining nowadays an increased interest, especially, DC microgrids. Many merits over AC grids, such as ease of control, higher efficiency and reliability…, make DC microgrid applications spread worldwide. Several researches address the control hierarchy and strategy in DC microgrids. On a local control level, Droop Control is a commonly used technique that ensures simultaneously DC bus voltage regulation and proper load sharing between operating converters. Yet, this paper investigates DC Microgrids control strategy from a different approach which is convenient, fundamentally, for remote islanded DC Microgrids. In such applications, the existence of the energy storage system (ESS) is substantial for a safe and stable Microgrid operation, especially, due to the intermittency and unpredictability of renewable energy sources (RESs) generated power. Hence, this paper proposes a simple, local control level, technique which is applied to a standard islanded DC Microgrid topology including: RESs, ESS and a back-up Diesel Generator (DG) as a traditional polluting source. The adopted control strategy main goal is to stabilize DC bus voltage, through ESS, and prevent battery excess discharge by connecting, temporarily, a back-up DG to the Microgrid as an additional source. When connected to the common DC bus, the DG takes charge of stabilizing the DC bus voltage. Once the power flow balance equation is reached again, the DG is disconnected instantly in order to reduce Carbone emissions. Finally, simulation tests are conducted in order to prove the viability and robustness of the proposed method.**

I. INTRODUCTION

In recent decades, there has been increased interest in renewable energy sources, which can be an alternative to traditional sources of polluting energy such as coal, oil, natural gas, etc. which are being depleted and the cause of global warming. The use of renewable energy sources is growing rapidly, which allowed to adopt a new approach of distributed architectures and to stand out from the conventional approach of centralized generation [1]. The distribution and connection of distributed sources to the conventional utility grid has been the subject of several studies over the past ten years, especially when these generators based on renewable energy sources are of different and intermittent nature, which poses a problem of energy quality when considering energy variations, voltage stability problems (voltage drop, rapid fluctuation, interruption, harmonic distortions…) [2].

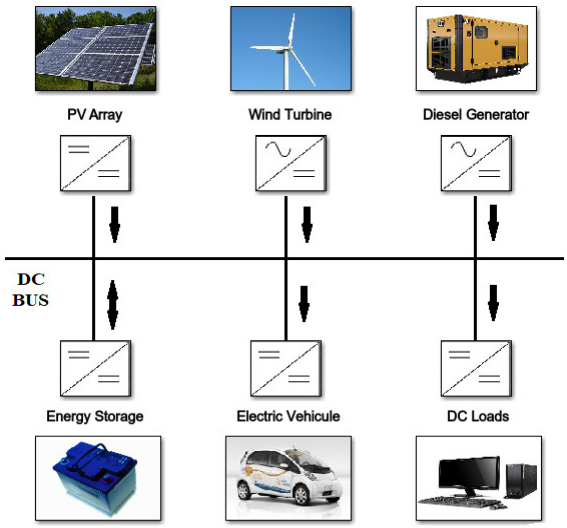

Fig.1 . Islanded DC microgrid configuration

The concept of microgrid were proposed more than a decade ago (2002) as a solution to electrify remote areas and integrate Renewable Energy Sources (RESs) with Energy Storage Systems (ESSs) and different types of sensitive and no sensitive loads [3]. Microgrids could operate in islanded mode as well as in grid connected mode and based on the type of connection between its different components, one can identify three types of microgrids: AC, DC and hybrid AC-DC microgrids [4] - [5]. The topology and configuration of a microgrid define its possible operating modes and the best strategy of control to be adopted. A typical islanded DC microgrid configuration is depicted in Fig.1, it consists of RESs: a solar PV array, a wind turbine, a back-up Diesel Generator, an ESS and different types of DC loads.

Many studies and surveys address the control strategies and hierarchy in DC microgrids [11], [12]- [14]. On a local control level, droop control is one of the most commonly used method that ensures simultaneously DC bus voltage stabilization and current load sharing [6]. In [17], secondary and tertiary control levels were added to the traditional droop control in order to improve its robustness and enhance efficiency of the conversion system. However, this paper proposes a different control strategy for DC Microgrids more precisely, islanded DC Microgrids which mainly rely on the Energy Storage

System (ESS). EESs are instrumental in islanded topologies due to the intermittency and unpredictability of renewable energy sources. RESs generated power varies regularly which introduce permanent instability and disturbances on the DC bus voltage thereby, the EES interference is mandatory to re-impose the stable operation of the system.

The proposed control strategy consists of local control functions of converters such as (MPPT, current and voltage regulation loops…). In addition, an emergency diesel generator is integrated as a backup source, its main role is to intercept intermittently, when alerted, to prevent battery excess discharge and take charge of stabilizing temporarily the common DC bus voltage. Once the balance between the requested and generated power is reestablished, the diesel generator is disconnected instantaneously to mitigate the environmental damage resulting from its usage. Thus, the control strategy adopted in the frame of this work improves overall system stability and reliability, increases ESSs lifetime which reduces considerably the cost function of the storage system [18] and reduces as much as possible the diesel generator carbon emissions. The simulations are performed on MATLAB/Simulink.

This paper is organized as follows: In section II, the microgrid configuration and the strategy of control of each unit is represented. Simulation tests are performed In Section III. Finally, section IV concludes the paper.

II. MICROGRID CONFIGURATION AND STRATEGY OF CONTROL

Fig.1 shows the microgrid configuration adopted in the frame of this work: each unit is connected to the common DC bus through its own converter controlled locally. To model the microgrid's units and components, *'' Simpower Systems''* library in MATLAB/Simulink is used since it includes all RESs, ESSs and power electronics required blocks. As a global strategy of control, all RESs are functioning in MPPT mode while, the battery takes charge of regulating the DC bus voltage by charging/discharging processes. However, the diesel generator, as a polluting energy source, intervenes only when the battery discharges and reaches its minimum admissible state of charge SOC_{min}. Moreover, if the Diesel Generator encounters any failure while connected to the Microgrid, load shedding would be the only remaining option to ensure system stable operation. We take note that load shedding and fully charged battery mode are out of the scope of this paper. In the following, each microgrid unit and converter strategy of control are represented apart:

A. PV Array

'' PV array'' block, from *"SimScape"* library, is used to model the PV solar generation. Based on current and voltage equations (I) and (II), the P-*V* characteristic for a PV array is defined by equation (III):

$$I_{PV} = I_L - I_0\left[exp\left(\frac{V_d}{V_T}\right) - 1\right] - I_{sh} \quad \text{(I)}$$

$$V_{PV} = V_d - R_s.I_{PV} \quad \text{(II)}$$

$$P(V_{PV}) = \mathrm{I_{PV}} \times \mathrm{V_{PV}} = \mathrm{V_{PV}} \times \mathrm{I}_L - \mathrm{V_{PV}} \times \mathrm{I}_0\left[exp\left(\frac{V_{PV} + \mathrm{R_s}.\mathrm{I_{PV}}}{V_T}\right) - 1\right] - \mathrm{V_{PV}} \times \mathrm{I}_{sh} \quad \text{(III)}$$

Where $I_{PV}, I_L, I_0, V_d, V_T, I_{sh}, V_{PV}$ and R_s are respectively: PV current (A), light generated current(A), diode saturation current (A), diode voltage (V),temperature voltage (V), Shunt resistance current (A), PV voltage (V) and series resistance (Ω). For a fixed value of irradiation (W/m^2) and temperature (°C), $P(V_{PV})$ function is plotted and obtained curve shows the existence of a maximum power point. Hence, MPPT objective is to always track this maximum for different irradiances and temperatures conditions. The PV array, generating DC power by nature, is connected to the common DC bus voltage trough a DC/DC Boost converter functioning in MPPT mode. Many MPPT techniques were adopted in order to extract the maximum available power from the PV. The technique adopted in the frame of this work is the Perturb & Observe algorithm. As principle, The P&O algorithm uses a predefined increment value (Δd) which varies the duty cycle (D). The duty cycle is incremented/ decremented depending on the PV voltage and power variation signs (dV_{PV} & $dP(V_{PV})$). The algorithm is repeated whenever $dP(V_{PV}) \neq 0$, it converges once $dP(V_{PV}) = 0$ is reached. The last computed duty cycle value (D_{MPPT}), corresponds to the maximum PV power generation (P_{PV_max}).

B. Wind Turbine

The applied wind turbine configuration is shown in fig.2. a. It's a typical configuration [16] and consists of: a wind turbine model, a permanent magnet synchronous generator (PMSG),

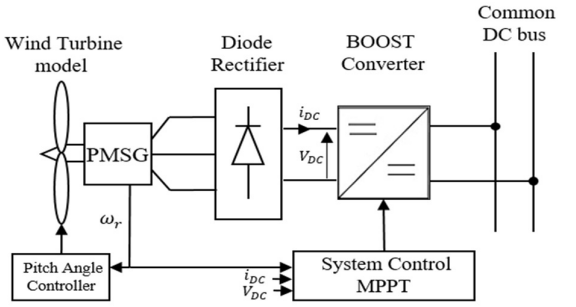

Fig.2. a. Wind Turbine Configuration

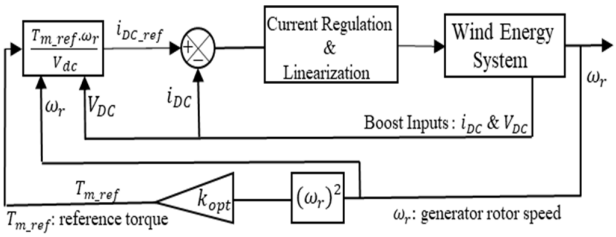

Fig.2. b. Block diagram of optimal torque control MPPT method

an uncontrolled Diode rectifier, a controlled DC/DC Boost converter connected to the common DC bus. Regarding the control strategy: a pitch angle controller block regulates the pitch angle of the turbine model and a system control block, consisting of a MPPT function, extracts the maximum available wind power. Several MPPT algorithms for wind turbines were reviewed in [19] such Tip speed ratio (TSR) control, Optimal torque (OT) control, Power signal feedback (PSF) control and Perturbation and observation (P&O) control. These methods were analyzed and compared in terms of simplicity, accuracy, flexibility… Due to its ease of implementation, the optimal torque control (OT) were applied as a MPPT algorithm. The mechanical power generated by a wind turbine can be expressed as:

$$P_m = \frac{1}{2}\rho\pi R^2 V^3 C_P(\lambda,\beta) \quad \text{(IV)}$$

Where ρ, R, V, C_P, λ and β are respectively: air density (Kg/m^3), turbine radius (m), wind speed (m/s), power coefficient, tip speed ratio and blade pitch angle (degree). The tip speed ratio can be expressed as:

$$\lambda = \frac{w_m R}{V} \quad \text{(V)}$$

With w_m: wind turbine rotational speed.

Based on $C_P(\lambda,\beta)$ expression in [19], there is only one optimal point, corresponding to $\beta = 0$ & $\lambda = \lambda_{opt}$, where C_P is maximum (C_{P_max}). Hence when operating at these point (C_{P_max}), we guarantee the extraction of maximum available power at any wind speed.

By substituting (V) into (IV), the expression yields:

$$P_m = \frac{1}{2}\rho\pi R^5 \frac{w_m^3}{\lambda^3} C_P \quad \text{(VI)}$$

If the system is running at λ_{opt}, it means $C_P = C_{P\_max}$.Thus (VI) can be expressed as:

$$P_m = \frac{1}{2}\rho\pi R^5 \frac{C_{P\_max}}{{\lambda_{opt}}^3} w_m^3 = k_{opt}.w_m^3 \quad \text{(VII)}$$

Based on the mechanical generated power of the wind turbine $P_m = T_m.w_m \rightarrow T_m$ expression can be rearranged as follow:

$$T_m = k_{opt}.w_m^2 \quad \text{(VII)}$$

Where T_m is the mechanical torque of wind turbine ($N.m$).

As shown in fig.2.a, a permanent magnet synchronous machine (PMSG) is chosen as a generator to produce AC power. A high number of pair of poles machine is utilized which makes low speed/high torque operation allowable and avoids the usage of speed gearbox. Thus, Wind turbine output mechanical torque (T_m) and wind turbine rotational speed (w_m) are respectively equal to PMSG shaft mechanical torque (T_{m_PMSG}) and rotor mechanical speed (w_r).

Fig. 2.b. shows the block diagram of the (OT) MPPT method: Boost input current (i_{DC}) and voltage (V_{DC}) are measured and DC current reference is generated (i_{DC_ref}) based on the below power equality equation:

$$P_m = P_{elec} \rightarrow T_m.w_r = V_{DC}.i_{DC} \quad \text{(VIII)}$$

In MPPT mode, mechanical torque reference (T_{m_ref}) is computed using equation (VII):

$$T_{m\_ref} = k_{opt}.w_r^2 \quad \text{(IX)}$$

Finally, DC current reference expression is expressed as:

$$i_{DC\_ref} = \frac{T_{m\_ref}.w_r}{V_{DC}} \quad \text{(X)}$$

DC Boost input current is compared to its reference and regulated through a P.I, a linearization stage is required due to the Boost non-linearity gain and then, PWM generator produces firing pulses that control Boost switch.

C. *Diesel Generator*

Different mathematical models of Diesel Generator (DG) are mentioned in [15]. The dynamic model adopted in this study addressees the electrical aspects of a DG rather than the mechanical ones. As shown in fig.3. a., it consists of a Diesel Engine Governor block which includes a diesel engine modelled by a second order transfer function, and a governor system modelled by a P.I.D. controller which regulates the generator speed on a desired value. This block outputs the diesel engine mechanical power to be provided to the synchronous machine (SM).

In addition, an excitation system block exists, it implements a synchronous machine voltage regulator and exciter based on the IEEE excitation system model. The block output is the field voltage to apply to the input of a (SM). Thereby, DG output voltage and frequency are conventionally regulated. As mentioned before, the DG main role is to intercept intermittently and produce energy, as a backup source, when two conditions are satisfied: first, RESs generated power is less than the load demand. Second, the battery has already reached its minimum admissible discharge limit. In that case, the DG is connected to the common DC bus in order to balance the power flow and prevent battery excess discharge. Once the power deficit is no longer persistent, the DG is disconnected form the microgrid.

As shown in fig.3.a, the SM, generating AC power, is connected to the common DC bus through a controlled AC/DC 3Ø PWM Rectifier. Fig.3. b. shows the Simulink block diagram of the adopted control strategy: It can be seen, that a switch function is used to initiate (DG) connection to the common DC bus. One of the two output power references (P_{DG_ref1} , P_{DG_ref2}) is selected based on the bellow predefined criteria:

$$SOC \leq SOC_{min} \quad AND \quad P_{DG\_ref1} \geq P_{DG\_min}$$

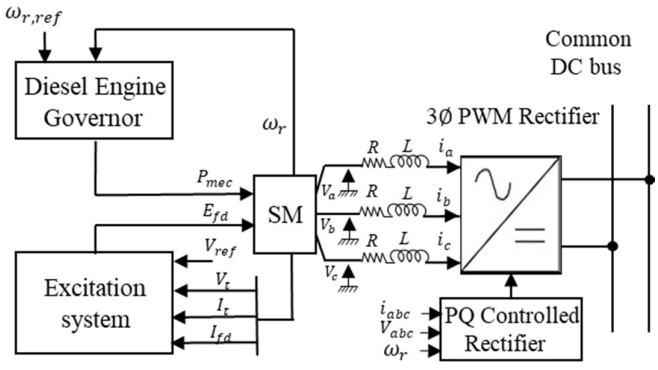

Fig .3.a . Diesel Generator Configuration

Where $SOC, SOC_{min}, P_{DG\_ref1}$ and P_{DG_min} are respectively: battery state of charge (%), battery minimum admissible state of charge(%), (DG) power reference (W), (DG) minimum generation power threshold (W). However, the reactive power reference ($I_{q\_ref} = 0$) is always set to zero.

Three different operating modes exist:

Mode 1:

RESs generated power is greater than the load demand, the battery stabilizes the DC bus voltage by absorbing the excess of generated power. In this mode, the battery is charging ($SOC > SOC_{min}$) so, the selected criteria is not satisfied which means that the switch is connected to the power reference 2 ($P_{DG\_ref2} = 0$ & $Q_{DG\_ref} = 0$). Hence, the converter is disabled and the (DG) is off.

Mode 2:

Contrarily, if the load demand is greater than the RESs power production ($\sum P_{Loads} > \sum P_{RESs}$), the battery switches to the discharging mode in order to cover the deficit of power generation and stabilize the common DC bus voltage. This operating mode remains whenever the battery doesn't reach its minimum discharging threshold (SOC_{min}).

Mode 3:

When discharging, the battery reaches its minimum admissible state of charge ($SOC \leq SOC_{min}$), the switch passes through power reference 1 which initiates DG connection to the microgrid and set the power reference equal to:

$$P_{DG\_ref1} = \sum P_{Loads} - \sum P_{RESs}$$

By this, the (DG) intercepts, as an additional power source, and provides the rest of unavailable load power demand. Thus, the battery switches to a floating mode with a zero-circulating current ($I_{Batt} = 0$) and consequently, the discharging process is stopped, the battery SOC is stabilized on its minimum allowable threshold (SOC_{min}). Finally, once RESs generated power climbs and surpasses the total load demand, the system switches again to operating *mode 1* and DG is shut down.

P. S: In order to ensure a standard Diesel Generator operation, a (DG) minimum generation power threshold is defined (P_{DG_min}).The (DG) generated power must be always greater than this minimum threshold. For that, the (DG) is disconnected from the DC bus voltage (in Mode 3) before the exact establishment of microgrid power balance ((DG) disconnected when $\sum P_{Loads} - \sum P_{RESs} = P_{DG\_min}$).

Fig.3. c. shows the block diagram of the applied (DG) dq

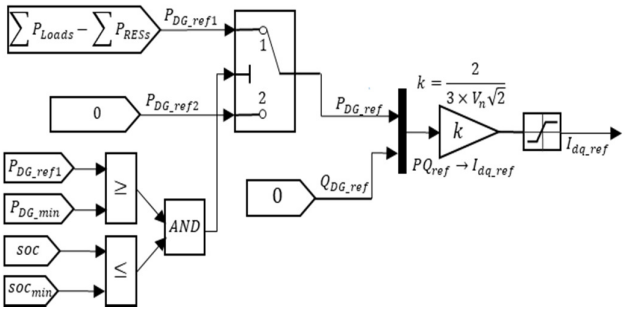

Fig.3. b. Simulink Block diagram of (DG) power references strategy

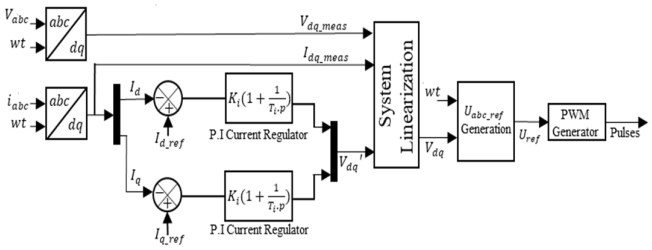

Fig.3. c. Simulink Block diagram of (DG) dq power control

power control: (DG) converter controls the synchronous machine output power through d axis (direct current component: I_d) and reactive power through q axis (quadratic current component: I_q). As previously mentioned, $P_{DG\_ref} \rightarrow (I_{d\_ref})$ is set based on the predefined criteria while, $Q_{DG\_ref} \rightarrow (I_{q\_ref} = 0)$ is set to zero in order to obtain a unit power factor. The generated (dq) current references are compared to the measured ones and regulates through P.I controllers. Then, a system linearization block is required before the generation of the converter voltage references. The linearization equations are expressed as follows:

$$V_d = V_{d\_meas} + L.w.I_q - R.I_d - L.\frac{dI_d}{dt} \qquad (XI)$$

$$V_q = V_{q\_meas} - L.w.I_d - R.I_q - L.\frac{dI_q}{dt} \qquad (XII)$$

Where,

$V_d, V_q, V_{d\_meas}, V_{q\_meas}, I_d, I_q$, w, L and R are respectively: converter d-axis voltage reference (V), converter q-axis voltage reference (V), (DG) d-axis measured voltage (V), (DG) q-axis measured voltage (V), (DG) d-axis measured current (A), (DG) q-axis measured current (A), (SM) electrical velocity (rd/s), coupling inductance (H) and coupling resistance (Ω). Linearization block outputs converter (dq) reference voltages then, a $(dq) \rightarrow (abc)$ transformation is accomplished in order to obtain three phases converter voltage references (V_{abc_ref}). Finally, switches pulses are generated through PWM Generator block.

D. Battery and DC loads

The ''Battery'' block is used to implement a Lithium-Ion battery model. It's connected to the DC bus voltage through a DC/DC bidirectional converter which functions as Boost in discharging process and as Buck in charging process. The battery main control objective is the regulation of the common DC bus voltage. A cascaded voltage and current loops regulation technique is adopted as shown in fig.4: the DC bus voltage is regulated using a P.I. controller which generates the reference current to be injected/absorbed from the battery, then

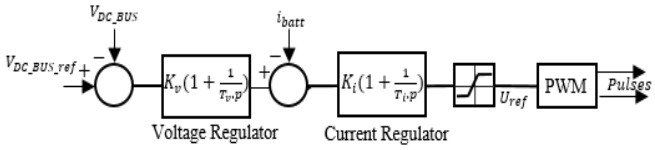

Fig.4. Battery cascaded loop regulation

the battery current is regulated using another P.I (*All P.I.s are*

equipped with Anti-Windup systems). However, variable DC current sources are utilized to model the DC loads.

III. SIMULATION TESTS AND RESULTS

Two Simulation tests are performed to prove the viably and the robustness of the proposed control strategy: First, overall system is tested apart in operating Mode 1*((DG) is disconnected)*. In this simulation, the MPPT algorithms convergency and the common DC bus voltage stability are verified. However, the second simulation test highlights the transition between prementioned operating modes and tests the robustness of the overall system towards sources and load power profiles variations. Microgrid parameters and data are listed in table 1. It is worth mentioning that, average model converters blocks are adopted in both simulations' tests. By using this approach, converters are modelled by switching-functions instead of real switching devices which make it directly controllable by the duty cycle signal. Hence, PWM generator is not required which increases Simulation step size and speed. As a result, DC Microgrid proposed control strategy and different operating modes could be tested over a wider range of time.

Simulation test 1:

In this simulation, the DC Microgrid is operating in Mode 1. Fig.5. a, 5.b and 5.c, show the PV array irradiance profile, the generated power and the MPPT convergence algorithm. It's shown that generated power is proportional to the irradiance (E_e) with a maximum PV generation of ($P_{pv\_max} = 100.5\ KW$) for ($E_e = 1000\ W/m^2$) and a minimum of ($P_{pv\_min} = 22.6\ KW$) for ($E_e = 250\ W/m^2$).

P&O algorithm convergency is verified through $dP(V_{PV})/dV_{PV}$ expression. Knowing that MPPT is reached if $dP(V_{PV})/dV_{PV}$ is equal to zero, one can conclude the following expression:

$$dP(V_{PV})/dV_{PV} = d(V_{PV} \times I_{PV})/dV_{PV} = 0$$
$$\Rightarrow dI_{PV}/dV_{PV} = -I_{PV}/V_{PV}$$

dI_{PV}/dV_{PV} and $-I_{PV}/V_{PV}$curves are plotted in Fig. 5.c. It's is shown that both curves are merged which means that the maximum power point is always tracked and hence, the P&O algorithm converges.

Wind turbine power characteristics are depicted in Fig.6. For each wind speed (m/s) corresponds a wind power curve (W) depending on turbine speed (rd/s). Furthermore, each power curve has a maximum of wind power generation to be tracked by the optimal torque MPPT control. Results of wind turbine generation are illustrated in Fig. 7. a., b. and c., three wind speed inputs are set ($V = 12\,m/s\,, 9.6\,m/s$ and $10.8\ m/s$). From Fig.6, maximum power generation and corresponding turbine speed for each of the predefined wind speed inputs can be drawn as follows:

- $V_1 = 12\,m/s : (P_{m\_max} = 0.8\,p.u,\ w_r = 1\,p.u)$
- $V_2 = 9.6\,m/s : (P_{m\_max} = 0.4\,p.u,\ w_r = 0.8\,p.u)$
- $V_3 = 10.8\,m/s : (P_{m\_max} = 0.58\,p.u,\ w_r = 0.9\,p.u)$

It can be seen by Fig. 7.b. and .c, that generated power follows the predefined maximum power values. Moreover, the corresponding wind turbine speeds are equal to the prementioned ones which implies that, Optimal Torque MPPT method converges and maximum wind power tracking is well achieved. Finally, Fig 8.a and b. show respectively DC microgird power flow and common DC bus voltage variations. In Fig 8.a, load power demand drops from $P_{load} = 36KW$ to $22\ kW$ at $t = 30\ s$ then, steps up to $50.3\ KW$ at $t = 50\ s$. Battery power curve (*blue curve*) is negative during all the simulation which means that DC Microgrid is operating in Mode 1, the battery is in charging mode and absorbs the excess of RESs generated power in order to stabilize the DC Bus voltage. Power flow balance equation ($P_{Batt} = \sum P_{Loads} - \sum P_{RESs}$) is always verified which ensures a stable operation of the common DC Bus voltage (Fig.7.b) within the allowable limits.

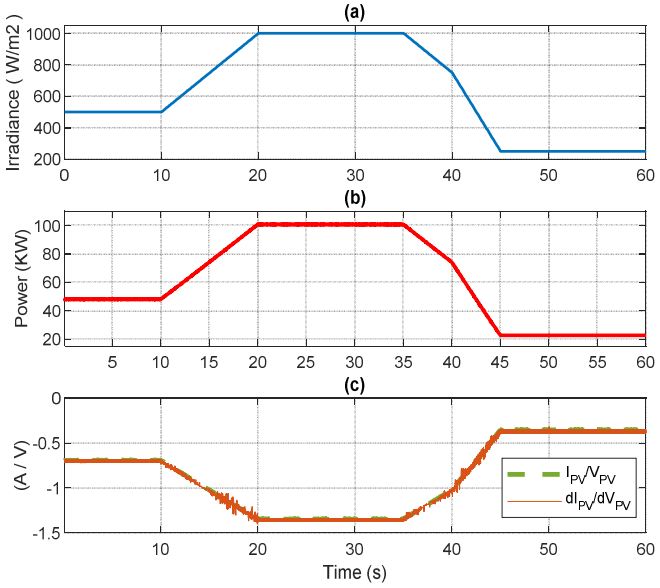

Fig.5. PV array (a) irradiance (w/m2), (b) Generated power (KW), (c) MPPT P&O algorithm convergency test (A/V)

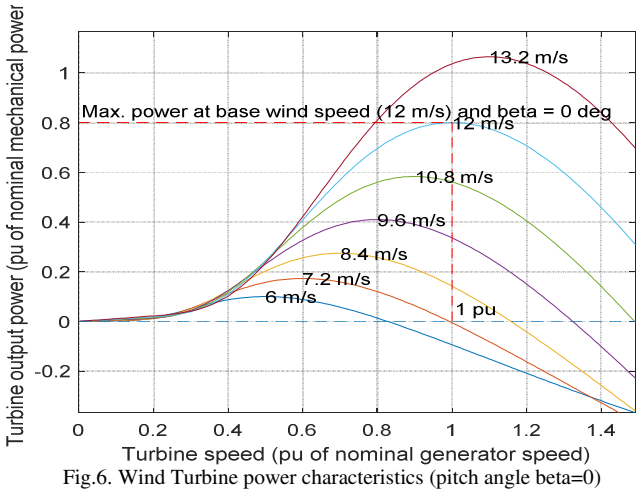

Fig.6. Wind Turbine power characteristics (pitch angle beta=0)

Hence, DC Microgrid stable operation is verified for steep and simultaneous sources and load profiles variations.

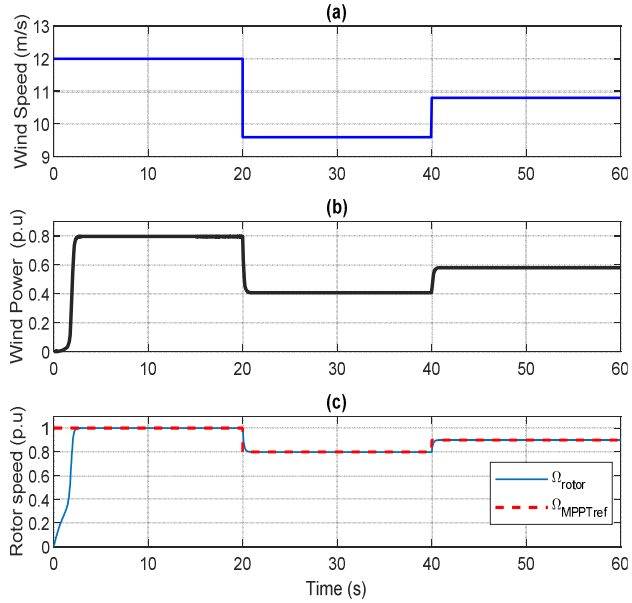

Fig.7. Wind Turbine (a) Input speed (m/s), (b) Generated power (p. u), (c) Rotor Speed and reference (p. u)

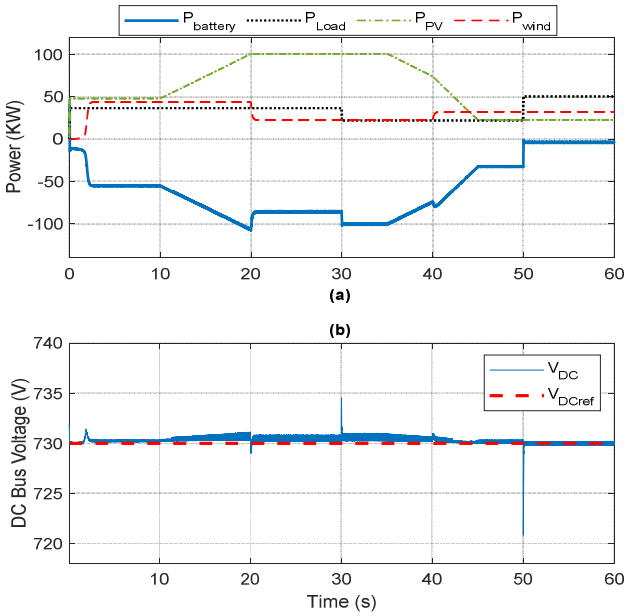

Fig.8. DC Microgrid (a) Power flow (KW), (b) Common DC Bus voltage and reference (V)

Simulation test 2:

In this simulation, Microgrid different operating modes are tested. The proposed (DG) intercepting method and DC Microgrid stable operation are validated. A (600s) simulation is conducted in order to test all system operating modes and prove the robustness and stability of the proposed control strategy over wide time ranges. It's shown by Fig.9.a, that RESs and load power profiles are all variables throughout the entire simulation. Constantly functioning in MPPT mode, RESs total generated power is insufficient to meet load high power demand at simulation starting point ($P_{Load} > \sum P_{RESs}$). Hence, the system is initialized in operating *(Mode 2)*. While operating in this mode ($0s < t < 269\ s$), the battery discharges in order to balance Microgrid power equation and stabilize the DC bus voltage. Battery discharging process is shown in Fig. 9. a and 10. a: battery power curve (*blue curve*) remains positive during this mode ($P_{battery} > 0$) and SOC

Common DC Bus rated voltage		$730\ V$
Allowable DC bus voltage continuous deviation		$\pm\ 10\%$
Allowable DC bus voltage cyclic fluctuation		$\pm\ 5\%$
Wind turbine maximum rated power		$55\ KW$
PV array maximum rated power		$100.7\ KW$
(DG) Rated Parameters	Power (KW) - frequency (Hz)	$55\ KW$ - $50\ Hz$
	Nominal voltage $V_n(ph-ph)$	$380\ V$
	$P_{DG\ min}\ (KW)$	$5\ KW$
Maximum rate of change of reference (DG) power		$1\ p.u/s$
Battery rated capacity and voltage		$500\ Ah - 300\ V$
Battery minimum admissible state of charge		$SOC_{min} = 30\%$
(DG) rectifier current Regulators gains		$T_i = 0.0013$ $K_i = 0.7$
(WT) Boost current Regulator gains		$T_i = 0.002$ $K_i = 26.4$
Battery converter voltage Regulator gains		$T_v = 350$ $K_v = 7.5$
Battery converter current Regulator gains		$T_i = 0.5$ $K_i = 0.1$

Table 1. DC Microgrid parameters and data

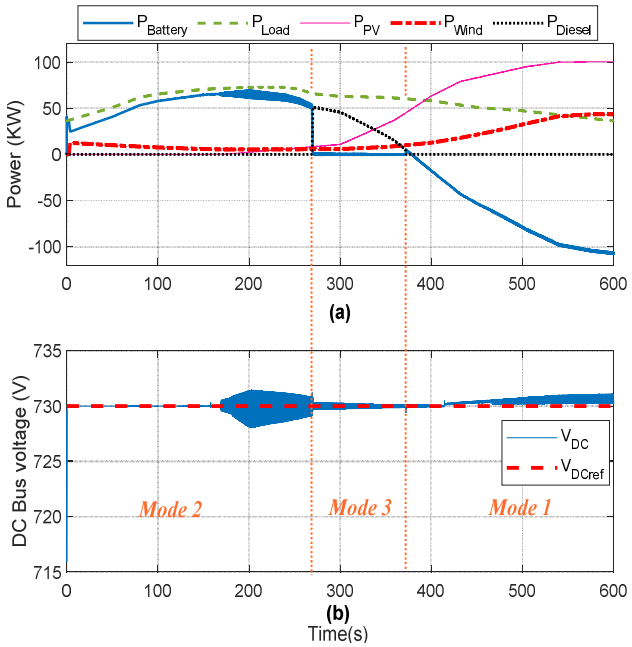

Fig .9. DC Microgrid (a) Power flow in different operating modes (KW), (b) Common DC Bus voltage and reference (V)

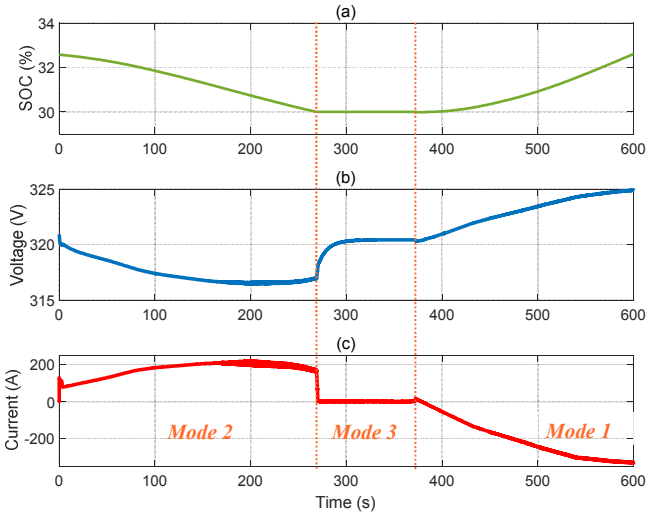

Fig.10. Battery (a) SOC (%), (b)Voltage (V), (c) Current (A)

decreases progressively from ($SOC_{init} = 32.65\ \%$) at $t = 0\ s$ ($SOC_{min} = 30\ \%$) at $t = 269\ s$.

However, (DG) is disconnected from the Microgrid. Fig.9. a. shows that (DG) power curve is null ($P_{Diesel} = 0$) *(Black dotted curve)*. Similarly, Fig.11.a illustrates (DG) (d q) currents components which are both null at this Mode. Thus, (DG) switching function is set to power reference 2 ($P_{DG\_ref2} = 0\ , Q_{DG\_ref} = 0$). At $t = 269\ s$, battery SOC reaches its minimum admissible value ($SOC_{min} = 30\%$). Hence, system switches from operating (*Mode 2*) to (*Mode 3*) and (DG) is connected to the Microgrid throughout the common DC Bus as an additional power source. P_{Diesel} rises from zero at ($t = 269\ s$) to its predefined power reference 1($P_{DG\_ref1} = \sum P_{Loads} - \sum P_{RESs}\ , Q_{DG\_ref} = 0$).

By connecting the (DG), power balance equality is always established, and DC bus voltage stable operation is maintained (Fig.9.b). Therefore, $P_{battery}$ drops, immediately, to zero and SOC downfall is stopped and stabilized on its minimum allowable threshold ($SOC_{min} = 30\%$). Consequently, the battery switches to a floating mode, with a zero current ($I_{Batt} = 0$ - Fig.10.c), and discharging process is interrupted. Mode 3 is hold whenever load power demand exceeds RESs power production. Then, RESs generated power increases progressively so, the gap between generated and demanded power is reduced and reaches ($\sum P_{Loads} - \sum P_{RESs} = P_{DG\_min}$) at $t = 376\ s$. Thus, DG switching functioning power reference 2 is enabled and the DG is disconnected from the grid. Consequently, DC Microgrid switches to operating (*Mode 1*). Battery switches to charging mode in order to maintain DC Bus voltage stability. Charging mode is illustrated in Fig.9.a and Fig 10.c: For $t > 376\ s\ I_{battery} < 0$ & $P_{battery} = \sum P_{Loads} - \sum P_{RESs} < 0$. Additionally, battery SOC increases from($SOC_{min} = 30\ \%$) to 32.5% at $t = 600\ s$.

Fig.9. b. shows a stable DC bus voltage operation over all the simulation and a smooth transition between different operating Modes. (DG) synchronous generator rotor speed and AC

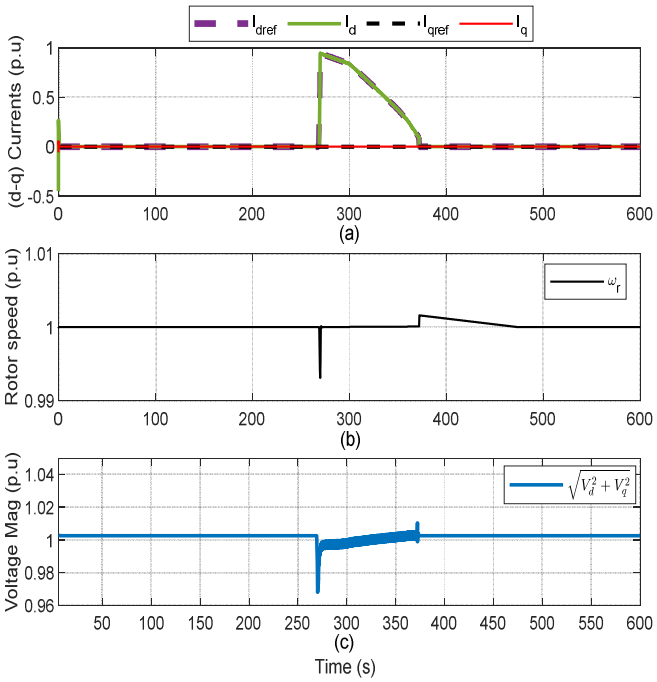

Fig.11. DG (a) (d q) currents components (p. u), (b) Synchronous Generator rotor speed (p. u), (c) AC output voltage Magnitude (p. u)

output voltage Magnitude, depicted in Fig.11, are well regulated on their rated references and represent a stable performance throughout the entire simulation. Finally, DG d-q current components follow their references: d-axis corresponds to the active power generation (KW), based on the prementioned power references switching criteria while, q-axis corresponds to the reactive power generation (KVAR). I_q is always null, as predefined, in order to obtain a unit power factor.

IV. CONCLUSION

In this paper, an islanded DC microgrid control strategy is proposed. A typical remote islanded Microgrid configuration is selected, it includes: RESs, ESS, DC loads and a back-up Diesel Generator as polluting source. The proposed method aims to stabilize the common DC bus voltage, extend battery lifetime by preventing its excess discharge and reduce, as possible, DG carbon emission. A predefined switching function enables DG connection to the Microgrid. Hence, three different DC Microgrid operation modes are distinguished. Control of parallel converters consists of primary level local control functions (MPPT, Current, voltage loops regulations, …). Simulations were conducted on MATALB/Simulink platform. In order to prove the viability and robustness of the proposed control strategy, microgrid different operating modes were tested over wide time range simulation and variable sources and load power profiles. Results show a stable Microgrid operation and smooth transition between different operating modes.

ACKNOWLEDGMENTS

The authors gratefully thank the Lebanese National Council for Scientific Research (CNRS-L) and the PHC CEDRE 2020 Project for their financial support.

REFERENCES

[1] F. Katiraei, R. Iravani, N. Hatziargyriou, and A. Dimeas, "Microgrids management," IEEE Power Energy Mag., vol. 6, no. 3, pp. 54–65, 2008.

[2] A. Ipakchi and F. Albuyeh, "Grid of the future," IEEE Power Energy Mag., vol. 7, no. 2, pp. 52–62, Mar./Apr. 2009.

[3] R. Lasseter, A. Akhil, C. Marnay, J. Stevens, J. Dagle, R. Guttromson, A. S. Meliopoulous, R. Yinger, and J. Eto, "The certs microgrid concept—White paper on integration of distributed energy resources," U. S. Department of Energy, Washington, DC, USA, Technical Rep., 2002.

[4] R. H. Lasseter, "Microgrids and distributed generation," J. Energ. Eng., vol. 133, no. 3, pp. 144–149, 2007.

[5] J.M. Guerrero, J.C. Vasquez, J. Matas, L.G.de Vicuna, and M. Castilla, "Hierarchical control of droop-controlled AC and DC microgrids—A general approach toward standardization," IEEE Trans. Ind. Electron., vol. 58, no. 1, pp. 158–172, Jan. 2011.

[6] J. C. Vasquez, J. M. Guerrero, A. Luna, P. Rodriguez, and R. Teodorescu, "Adaptive droop control applied to voltage-source inverters operation in grid-connected and islanded modes," IEEE Trans. Ind. Electron., vol. 56, no. 10, pp. 4088–4096, Oct. 2009.

[7] Donald J. Hammerstrom, "*AC versus DC distribution systems Did we get it right?"* 2007 IEEE Power Engineering Society General Meeting

[8] T. Dragicevic, J. C. Vasquez, J. M. Guerrero, and D. Skrlec, "Advanced LVDC electrical power architectures and microgrids: A step toward a new generation of power distribution networks," IEEE Electrif. Mag., vol. 2, no. 1, pp. 54–65, Mar. 2014.

[9] S. Parhizi, H. Lotfi, A. Khodaei, and S. Bahramirad, "*State of the art in research on microgrids: A review,*" IEEE Access., vol. 3, pp. 890–925, Jul. 2015.

[10] Tomislav Dragičević; Xiaonan Lu; Juan C. Vasquez; Josep M. Guerrero, "*DC Microgrids—Part I: A Review of Control Strategies and Stabilization Techniques*," IEEE Transactions on Power Electronics, 2016.

[11] Saroja Kanti Sahoo ; Avinash Kumar Sinha ; N. K. Kishore "*Control Techniques in AC,DC and Hybrid AC-DC Microgrid : A Review*" IEEE Journal of Emerging and Selected Topics in Power Electronics, Year: 2018 , Volume: 6 , Issue: 2

[12] S. Anand, B. G. Fernandes, and J. M. Guerrero, "Distributed control to ensure proportional load sharing and improve voltage regulation in low-voltage DC microgrids," IEEE Trans. Power Electron., vol. 28, no. 4, pp. 1900–1913, Apr. 2013.

[13] Q. Shafiee, T. Dragicevic, J. C. Vasquez, and J. M. Guerrero, "Hierarchical control for multiple DC-microgrids clusters," IEEE Trans. Energy Convers., vol. 29, no. 4, pp. 922–933, Dec. 2014.

[14] T. Dragicevic, J. M. Guerrero, and J. C. Vasquez, "A distributed control strategy for coordination of an autonomous LVDC microgrid based on power-line signaling," IEEE Trans. Ind. Electron., vol. 61, no. 7, pp. 3313–3326, Jul. 2014.

[15] S. Benhamed *et al.*, « Dynamic modeling of diesel generator based on electrical and mechanical aspects », in *2016 IEEE Electrical Power and Energy Conference (EPEC)*, 2016, p. 1□6.

[16] H. Xu, J. Hui, D. Wu, W. Yan, et H. Xu, « Implementation of MPPT for PMSG-based small-scale wind turbine », in *2009 4th IEEE Conference on Industrial Electronics and Applications*, 2009, p. 1291□1295.

[17] Lexuan Meng, Tomislav Dragičević, J. M. Guerrero and J. C. Vasquez, "*Optimization with System Damping Restoration for Droop Controlled DC-DC Converters*" 2013 IEEE Energy Conversation Congress and Exposition.

[18] Inam Ullah Nutkani, Wang Peng, Poh Chiang Loh, and Frede Blaabjerg*" Cost-based droop scheme for DC microgrid"* 2014 IEEE Energy Conversion Congress and Exposition (ECCE)

[19] Abdullah M.A., Yatim A.H.M., Tan C.W., Saidur R., "*A review of maximum power point tracking algorithms for wind energy systems*" Renewable and Sustainable Energy Reviews, journal home page: www.elsevier.com/locate/rser

[20] E. Hleihel, M. Fadel and H. Y. Kanaan, "Simulation of an Islanded DC Microgrid Using Instantaneous and Average modeling approaches", in *Proc. 13th International Conference on Modeling and Simulation of Electric Machines, Converters and Systems (ELECTRIMACS'19)*, Salerno, Italy, May 21-23, 2019.

[21] S. Atanalian, M. Abarzadeh, H. Y. Kanaan and K. Al-Haddad, "PV Assisted EV Charging in DC Micro-Grids", in *Proc. 45th Annual Conference of the IEEE Industrial Electronics Society (IECON'19)*, Lisbon, Portugal, October 14-17, 2019.

[22] A. Hamadi, S. Rahmani, A. Ndtoungou, K. Al-Haddad and H. Y. Kanaan, "A New Maximum Power Point Tracking with Indirect Current Control for a Three-Phase Grid-Connected Inverter Used in PMSG-Based Wind Power Generation Systems", in *Proc. 38th Annual Conference of the IEEE Industrial Electronics Society (IECON'12)*, Montreal, Quebec, Canada, October 25-28, 2012, pp. 916-923.

[23] F. Sebaaly, H. Y. Kanaan and N. Moubayed, "A Comparative Evaluation of Conventional and Super-Capacitors in Grid-Connected Transformerless PV Systems", in *Proc. 19th IEEE International Conference on Emerging Technologies and Factory Automation (ETFA'14)*, Barcelona, Spain, September 16-19, 2014.